crystals

MDPI

Article

Synthesis and Experimental-Computational Characterization of a Copper/Vanadium Compound with Potential Anticancer Activity

Beatriz Martínez-Valencia [1], Nidia D. Corona-Motolinia [1], Eduardo Sánchez-Lara [1], Brenda L. Sánchez-Gaytán [1], Mónica Cerro-López [2], Angel Mendoza [1], María Eugenia Castro [1], Francisco J. Meléndez-Bustamante [3] and Enrique González-Vergara [1,*]

[1] Centro de Química del Instituto de Ciencias, Benemérita Universidad Autónoma de Puebla, 18 sur y Av. San Claudio, Col. San Manuel, C.P. 72570 Puebla,Mexico; beatriz.mvalencia@alumno.buap.mx (B.M.-V.); nidia.corona@alumno.buap.mx (N.D.C.-M); eduardo.sanchez@alumno.buap.mx (E.S.-L.); brendale.sanchez@correo.buap.mx (B.L.S.-G.); angel.mendoza@correo.buap.mx (A.M.); mareug.castro@correo.buap.mx (M.E.C.)

[2] Laboratorio de Ciencias Quimicobiológicas de la, Universidad de las Américas Puebla, Sta. Catarina Martir, Cholula 72820, Puebla, Mexico; monica.cerro@udlap.mx

[3] Facultad de Ciencias Químicas, Benemérita Universidad Autónoma de Puebla, 18 sur y Av. San Claudio, Col. San Manuel, C.P. 72570 Puebla, Mexico; francisco.melendez@correo.buap.mx

* Correspondence: enrique.gonzalez@correo.buap.mx

Received: 29 April 2020; Accepted: 2 June 2020; Published: 8 June 2020

Abstract: Cancer represents a major worldwide public health problem. While significant advances in different fronts are being made to combat the disease, the development of new metal-based drugs with cytotoxic capabilities is of high relevance. This work presents a heterobimetallic molecule comprising two moieties with a structure similar to Casiopeina II-gly. One of them has a cyclotetravanadate anion that functions as an inorganic bridge coordinating two Cu (II) atoms resulting in a hexanuclear $[Cu(phen)(Gly)\text{-}\mu2\text{-}V_4O_{12}\text{-}Cu(phen)(Gly)]^{2-}$ complex, which is counterbalanced by two isolated $[Cu(phen)(Gly)(H_2O)]^{1+}$ cations. Ten water molecules arranged in two sets of five-member chains also play an essential role in the 3D supramolecular structure of the compound. The molecule was designed to provide Cu and V, two metals with proven anticancer capabilities in the same molecular structure. The compound was synthesized and characterized by elemental analysis; visible, FTIR, and Raman spectroscopies; ^{51}V Nuclear Magnetic Resonance; cyclic voltammetry; and monocrystalline X-ray diffraction. The structural, spectroscopic, and electronic properties of the compound were calculated through the density functional theory (DFT) using the Minnesota functional M06-2X and the Def2TZVP/LANL2TZ(f) basis sets with an effective core potential (ECP) for metals. Noncovalent interactions were analyzed using a natural population analysis (NPA) and Hirshfeld surfaces. The compound upon dissociation provides two metals that can interact with important biological targets in a variety of cancer cell models.

Keywords: anticancer activity; copper; vanadium; glycine; 1,10-phenantroline; heterobimetallic compounds; DFT calculations

1. Introduction

Since the discovery of the strong chemotherapeutic properties displayed by platinum-based compounds, transition metal-based drug research has been subject to significant advances within the medical sciences [1]. Efforts towards the development of different transition metals-based drugs have grown due to the desire to avoid the adverse effects (e.g., neurotoxicity and nephrotoxicity) and

the resistance displayed by platinum-based drugs [2,3]. Among transition metals, vanadium and copper stand out since they both have shown more than one therapeutic use and have proven to be the basis of powerful metallodrugs [4]. Copper-based compounds have similar DNA damaging properties as platinum-based ones. They exhibit interesting anticancer properties, and contrary to other transition metal-based compounds, they can effectively be handled by the body, reducing unwanted side effects [5–7]. Transition metal complexes can interact with DNA in several ways, including intercalation, groove binding, and external electrostatic binding [8]. Molecular shape and conformation appear to be the most important aspects to determine the effectiveness of DNA binding, to the degree that even subtle conformation changes can impact the compound's pharmacological properties. Previous studies have shown that the square planar geometry exhibited by some metal centers, coupled with certain aromatic diimines acting as bidentate ligands, provides an optimal structure to interact with many biological molecules. Thus, this potentially makes them suitable as antitumoral and antiviral drugs [9]. The square plane geometry exhibited by both platinum and copper-based compounds seems to be ideal for DNA interaction and subsequent damage. However, in the case of copper-based compounds, the action mechanism also includes protease inhibition and the generation of reactive oxygen species (ROS) [10]. Additionally, the pharmacological properties and action mechanism of several copper (II) complexes that contain in their molecular structure planar moieties such as 1,10-phenanthroline and amino acids on cisplatin-resistant cancer (MDA-MB-231) and noncancer cells (MCF10A) have shown positive results solely against cancer cells [11]. Casiopeínas®, for instance, is a family of copper-based molecules whose molecular structure is optimal to interact with genetic material due to the presence of the planar moieties 1,10-phenanthroline or 2,2′-bipyridine and their derivatives, and it renders a metal center with a slightly distorted squared pyramidal structure. The mechanism of action of these compounds can involve diverse interference pathways in the cell cycle, turning them into powerful cytotoxic agents [12–16]. However, despite the encouraging in vitro results of copper-based therapeutics, there has been a limited transition to preclinical in vivo studies due in part to poor solubilities. The clinical trials of Casiopeínas® in Mexico is a step forward in the transition metal-based drugs field [17].

On the other hand, multiple therapeutic actions of vanadium have already been recognized, and its medicinal properties are currently the focus of considerable research around the world. Whereas the antidiabetic properties of vanadium are well known [18], its anticancer properties, which include the activation/inhibition of cancer mechanisms, have not been thoroughly investigated [19]. Due to its DNA binding and degradation capacities, vanadium-based compounds have shown novel anticancer properties [20–22]. Interestingly, there are similar metabolic pathways used by both diabetes and some kinds of cancer of which vanadium's behavior can take advantage [18,19,23]. Several studies of different types of vanadium-containing compounds displaying antineoplastic and cytotoxic effects identify its DNA cleavage and oxidation capabilities, as well as the ROS generated by the Fenton-like reactions during the intracellular reduction of V^{5+} to V^{4+} as the responsible factors for their antitumoral properties [24]. Thus, the redox behavior and the rich chemistry of vanadium-based compounds can be used to design new metallodrugs [25,26].

In the last two decades, some structures about the interactions of $[V_4O_{12}]^{4-}$ with metal-organic complexes have been reported. Searching in the CCDC database, 76 structures containing $[V_4O_{12}]^{4-}$ in different bridging modes or as a free anion were found. In 34 of them, the cyclotetravanadate anion bridges transition metals, and 10 of them are bridging Cu(II) cations (their codes are AGAGAR, VISNIV, VIWOEY, VIWOEY1, YENSUG, YENSUG01, and YENTOB). The typical organic ligand in these Cu complexes is 1,10-phenanthroline, together with bis-(2-pyridyl)-amine and recently with Lysine and Ornithine [27–32]. The last compounds [Cu(phen)(Lys)-μ2-V_4O_{12}-Cu(phen)(Lys)] and [Cu(phen)(Orn)-μ2-V_4O_{12}-Cu(phen)(Orn)], by the use of molecular docking studies, have shown to intercalate in DNA test fragments, thus opening the possibility of the development of potential heterobimetallic metallodrugs [32].

Considering that there were an estimated 18.1 million new cancer cases and 9.6 million cancer deaths in 2018 as a global health burden, it is relevant to find low cost and safe alternatives to combat cancer [33]. While the binding of metal ions with organic binders has proven useful for therapeutic purposes [34], in bimetallic compounds, the presence of the second metal introduces an additional potential active site. Therefore, the importance of synthesizing compounds with two highly important metal centers could produce drugs with dual anticancer properties. Here, we present a Cu/V heterobimetallic compound containing two pharmacological relevant transition metals. The structure comprises two types of copper sites, both containing pentacoordinate copper similar to Casiopeína II-Gly [35]. Two of them are bridged by a cyclotetravanadate moiety, generating an hexanuclear anion, which is neutralized by two cations of the formula [Cu(phen)(Gly)H_2O] that have already shown anticancer activity. Therefore, the new compound possesses both structural and biological relevance.

2. Materials and Methods

Ammonium metavanadate, 1,10-phenanthroline monohydrochloride, and glycine monohydrochloride were purchased from Sigma-Aldrich (Toluca, Mexico). KOH was purchased from Fermont, and $CuCl_2 \cdot 2H_2O$ was purchased from Química Dinámica S. A. de C. V. All manipulations were carried out at room temperature with no special solvent and reagent purification. Elemental analysis (EA) was carried out on a Perkin Elmer 2400 Series II CHNO/O Analyzer. The electronic spectrum of the complex was determined by UV-Vis spectroscopy with a Varian Cary 50 spectrophotometer with a xenon lamp and using a quartz cuvette of a 1 cm path length. The infrared spectrum was obtained in KBr pellets in a range from 400 to 4000 cm^{-1} by using an IR Digilab, Mod. Scmitar FTIR spectrophotometer. Raman spectra were obtained at room temperature in a backscattering configuration using the 633 nm line of a He-Ne laser as an excitation source by using a LabRAM HR-Olympus Micro Raman system. The ^{51}V-NMR spectrum was recorded at 131.5 MHz with a Bruker AVANCE III 500 MHz spectrometer using deuterated water (D_2O) and phosphate-buffered saline (PBS). Chemical shifts were referred to $VOCl_3$ as an external standard. Cyclic voltammetry experiments were performed in a three-electrode cell, with the platinum disk as the working electrode, the platinum wire as counter electrode, and Ag/AgCl/saturated KCl as a reference electrode. The electrolyte medium was a pH 7.4 phosphate buffer (0.1 M); it was deaerated before every cyclic voltammetry with nitrogen stream for 10 min, and this nitrogen stream was kept over the solution during experiments. Cyclic voltammetry was controlled with a DY2000 Series Multichannel Potentiostat (Digi-Ivy, Inc.). The complex concentration was 1.5×10^{-4} M, and *E. coli* plasmid DNA concentration was estimated to be between 5.5×10^{-10} to 1.8×10^{-9} M. The single-crystal structure analysis was carried out on an Agilent-Gemini diffractometer with a CCD Atlas detector with Cu radiation (λ = 1.54184 Å). Cell parameters were determined and refined using Crysalis PRO software [36]. Data reduction and absorption correction (analytical) were applied to the same software. The structure was solved by SHELXD and refined with SHELXTL (SHELX 2018/3) [37], utilizing OLEX2 [38]. No hydrogen atoms were refined anisotropically by full-matrix least-squares techniques. All hydrogens were placed geometrically and constrained to ride on their parent with Uiso(H) = 1.2Ueq and a C–H distance of 0.97 Å for methylene hydrogen atoms, 0.93 Å for aromatic hydrogen atoms, 0.89 Å for amino hydrogen atoms (N–H), and Uiso(H) = 1.5Ueq (O–H) for water hydrogen atoms with a 0.87 Å distance. The crystal structures were studied with Mercury CSD (release 4.0), which was also used to produce a crystallographic artwork [39].

2.1. Synthesis and Crystallization

The compound was prepared by a general synthesis method in which an aqueous solution was prepared with 1.0 mmol of 1,10-phenanthroline monohydrochloride (0.198 g) in 30 mL of distilled water with stirring and moderate heat. Once dissolved, 1.0 mmol of glycine (0.075 g) was added while stirring, followed by the addition of 1.0 mmol of $CuCl_2 \cdot 2H_2O$ (0.170 g). The mixture was allowed to cool to room temperature, and the pH was adjusted to 9.5 by adding some drops of a KOH solution

(10%). An aqueous solution of NH_4VO_3 (0.116g, 1.0 mmol in 15 mL of H_2O) was then added dropwise. Finally, the reaction mixture was filtered and left at room temperature for three days, obtaining deep blue prismatic crystals that were separated from any impurity and with sufficient quality to be used in the X-ray diffraction equipment. The following were obtained by elemental analysis (calcd.): C: 35.30 (35.71); N: 9.37 (8.93); H: 4.68 (3.8).

2.2. Theoretical Methodology

The molecular structure and electronic properties of the compound were computed from theoretical calculations based on the density functional theory (DFT) [40]. Since the compound exhibits two types of copper sites, it is possible that the ground state and their low-lying excited states do not follow a classic behavior. Relative and interaction energies of the different electronic states were computed by applying counterpoise correction [41,42] using single-point calculations. Subsequently, full optimization of the triplet electronic state of the compound was obtained using the global hybrid functional M06-2X [43], including 54% of Hartree-Fock (HF) exchange. Ultrafine integration grids, tight convergence criteria, and symmetry of the C_i point group were used. The stationary points (global minima) were identified by performing frequency calculations. The triple-ξ, and split-valence basis set Def2TZVP of Ahlrichs et al. [44,45] was used for C, H, O, and N atoms. A basis set LANL2TZ(f), which is suitable for the first, second, and third transition atomic series, was used [46–48]. The same effective core potential (ECP) was used for the V and Cu atoms. Implicit solvation was used with conductor-like polarizable continuum model (CPCM) [49] with water as the solvent. Additionally, a natural population analysis (NPA) [50,51] as well as IR and Raman spectra analyses were performed at the same theory level. Calculations were performed with the Gaussian16 program [52], and visualization of the results was carried out with the Gaussian View 6.0.16 program [53]. The Hirshfeld surface and the 2D-fingerprint plot were generated using CrystalExplorer 17.5 [54], obtained from the X-ray structure.

3. Results

The compound crystallizes at 294 K with 10 water molecules. The formula, as determined by X-ray diffraction is $[Cu(phen)(Gly)(H_2O)]_2[Cu(phen)(Gly)\text{-}\mu2\text{-}V_4O_{12}\text{-}Cu(phen)(Gly)]\cdot 10H_2O$. The condensed formula is $C_{56}\ H_{72}\ Cu_4\ N_{12}\ O_{32}\ V_4$. From now on, the compound will be named **Compound 1**.

3.1. Structure Description

Crystal data, data collection, and structure refinement details are summarized in Table 1. Fractional atomic coordinates and isotropic or equivalent isotropic displacement parameters (Å) and geometric parameters (Å, °) for **Compound 1** are presented in Tables S1 and S2 respectively in the supplementary material section. The crystal structure of **Compound 1** shows three components; one of them is a dicopper unit with the cyclotetravanadate anion acting as a bridge between two [Cu(phen)(Gly)]+ moieties, formed by two slightly distorted squared pyramidal complexes with (τ_5 = 0.20) [55], which are bound to two opposite oxygen atoms from the $[V_4O_{12}]^{4-}$ cluster, laid in the apical positions, which from now on is referred to as [Cu1]. As depicted in Figure 1. This unit is showing a −2 total charge. The second component is acting as a counterion [Cu2]. It consists of two slightly distorted squared pyramidal complexes $[Cu(phen)(Gly)(H_2O)]^+$ with (τ_5 = 0.06), where a coordinated water molecule is in the apical position. The third component is made by ten crystallization water molecules divided into two sets of five-member chains, which through hydrogen bonds construct a 3D supramolecular architecture of the compound. All metal-oxygen and metal-nitrogen distances are presented in Table 2. The packing in the unit cell is presented in Figure S1 in supplementary materials. The water molecules corresponding to O13 were located and included in the final refinement by considering two sites for each case (occupations = 0.79 and 0.21). The $[V_4O_{12}]^{4-}$ anion lies on an inversion center with four tetrahedral VO_4 units, each sharing two vertices, forming an eight-membered ring. Figure S2 shows the moiety containing the cyclotetravanadate ion acting as a bridge. The crystal packing is stabilized by face-to-face π–π interactions of the 1,10-phenanthroline aromatic rings in an alternated

layer along the c-axis, as seen in Figure 2. Distances from each phenanthroline centroids are 3.588, 3.692, and 3.802 Å, indicating the interlayer space. The Cu1–Cu2 distance is 5.730 (5) Å, as shown in Figure S3, and the Cu1–Cu1 distance is 11.019 (5) Å, which is not shown. Intermolecular hydrogen bonds play a fundamental role in the supramolecular structure of the compound, as shown in Figures 3–5. Twenty-four hydrogen bonds hold together a tridimensional array of [Cu1][Cu2] units (Table 3).

It is essential to point out that the water molecules play an important role in the stability of the complex, not only because of the intramolecular hydrogen bonds but also in the supramolecular structure build from intermolecular ones, as shown in Figures 3–5. These interactions are responsible for the low solubility of **Compound 1.**

The CCDC number assigned for the compound is **1996484**. This data can be obtained free of charge at http://www.ccdc.cam.ac.uk/conts/retrieving.html (or from the CCDC, 12 Union Road, Cambridge CB2 1EZ, UK; Fax: +44-1223-336-033; e-mail address: deposit@ccdc.cam.ac.uk).

Table 1. Selected crystal data and details of the structure determination for **Compound 1**.

Empirical Formula	**C_{56} H_{72} Cu_4 N_{12} O_{32} V_4**
Formula weight	1883.18
Temperature/K	293(2)
Crystal system	Triclinic
Space group	P−1
a/Å b/Å c/Å	11.9249(4) 13.2626(4) 13.5191(4)
α/° β/° γ/°	109.108(3) 95.685(3) 113.173(3)
Volume/$Å^3$	1792.27(10)
Z	1
δcalc g/cm^3	1.745
μ mm^{-1}	6.292
F(000)	956.0
Crystal size/mm^3	0.303 × 0.14 × 0.052
Radiation	Cu Kα (λ = 1.54184)
2Θ range for data collection/°	7.172 to 154.71
Index ranges	−15 ≤ h ≤ 14, −16 ≤ k ≤ 16, −16 ≤ l ≤ 17
Reflections collected	38143
Independent reflections	7587 [R_{int} = 0.0568, R_{sigma} = 0.0496]
Data/restraints/parameters	7587/0/514
Goodness-of-fit on F^2	1.046
Final R indexes [I > 2σ (I)]	R_1 = 0.0380, wR_2 = 0.0884
Final R indexes [all data]	R_1 = 0.0470, wR_2 = 0.0948
Largest diff. peak/hole / e $Å^{-3}$	0.46/−0.36

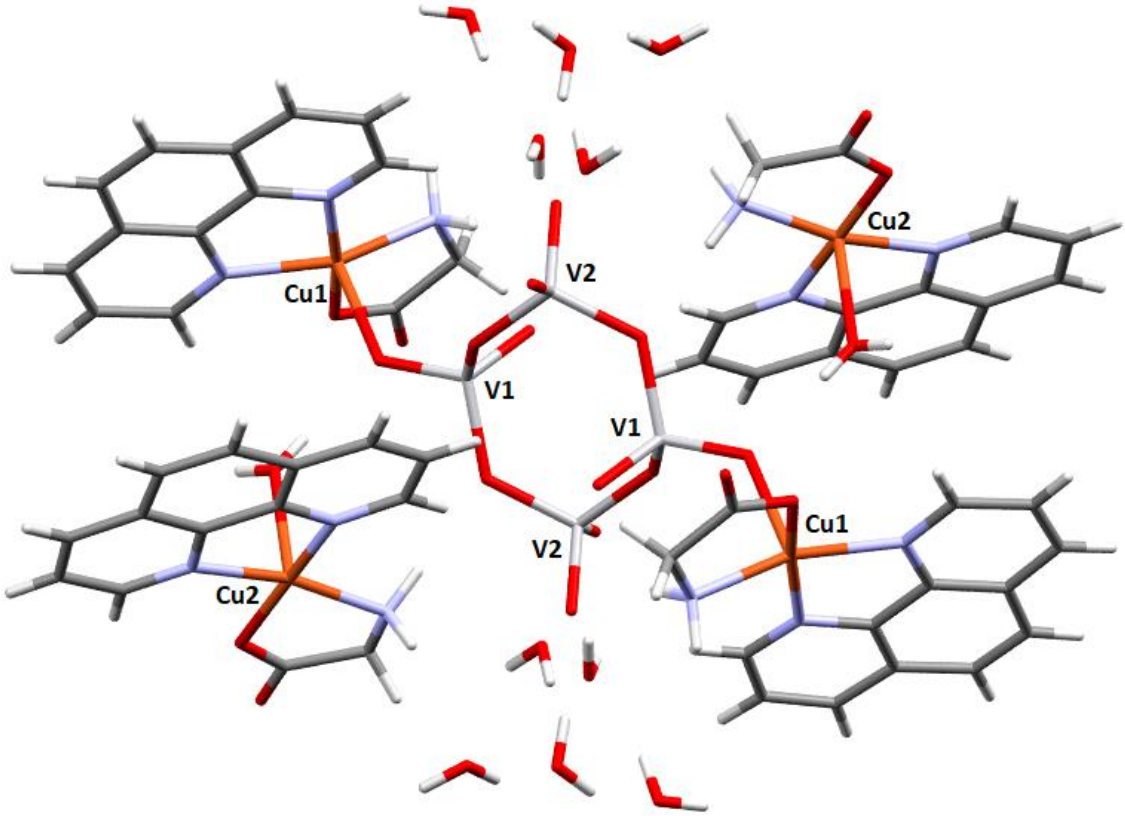

Figure 1. Capped stick representation of the molecular structure of **Compound 1.**

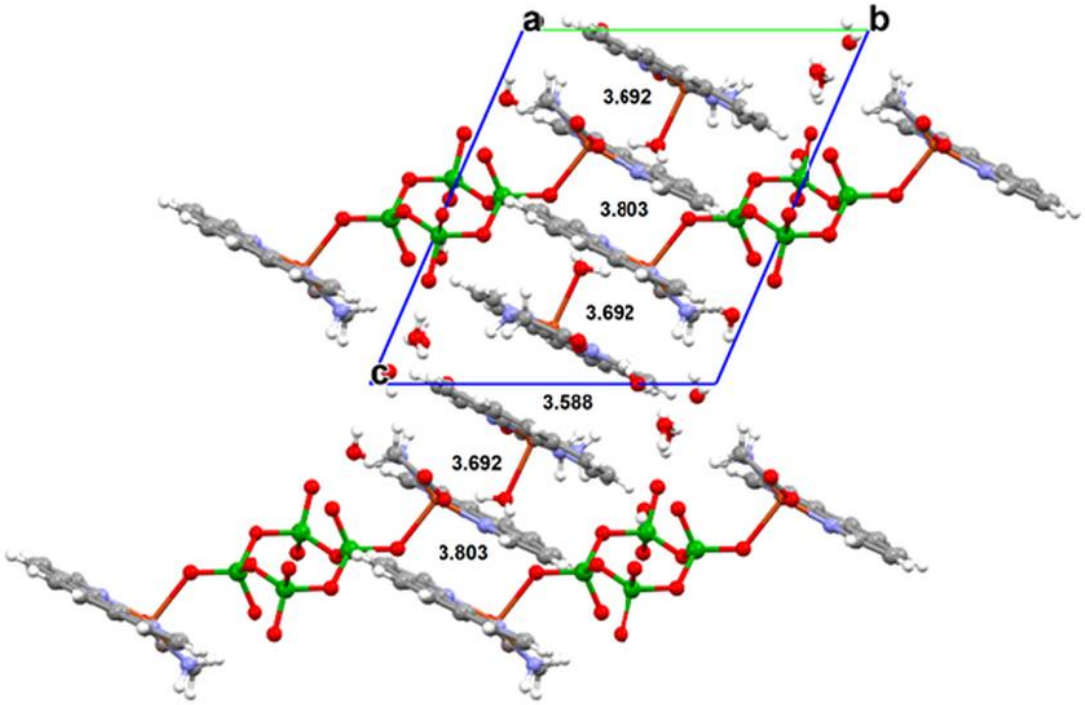

Figure 2. Ball and stick representation of the stacking of complexes in the structure of **Compound 1** along with the [0,1,−1] crystallographic direction through π–π interactions.

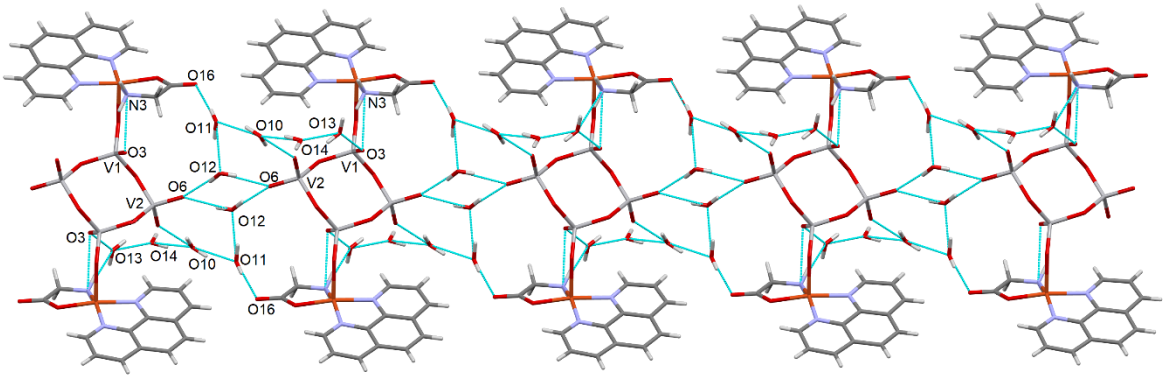

Figure 3. Capped stick representation of the hydrogen bond network that aligns all the cyclotetravanadate units in a monodimensional supramolecular structure along the a-axis. Red arrows point to truly intramolecular hydrogen bonds.

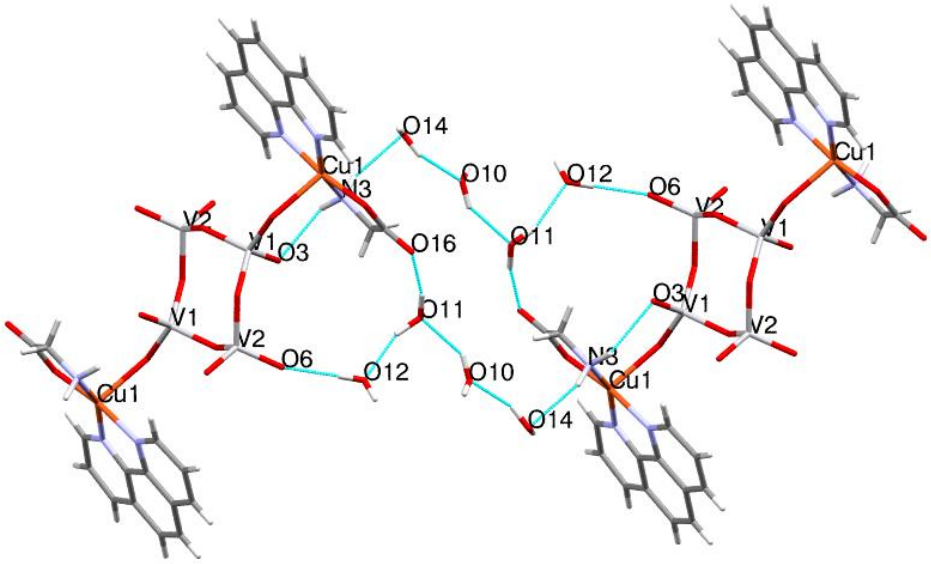

Figure 4. Capped stick representation of the hydrogen bond network communicating the cyclotetravandates in the *c* direction.

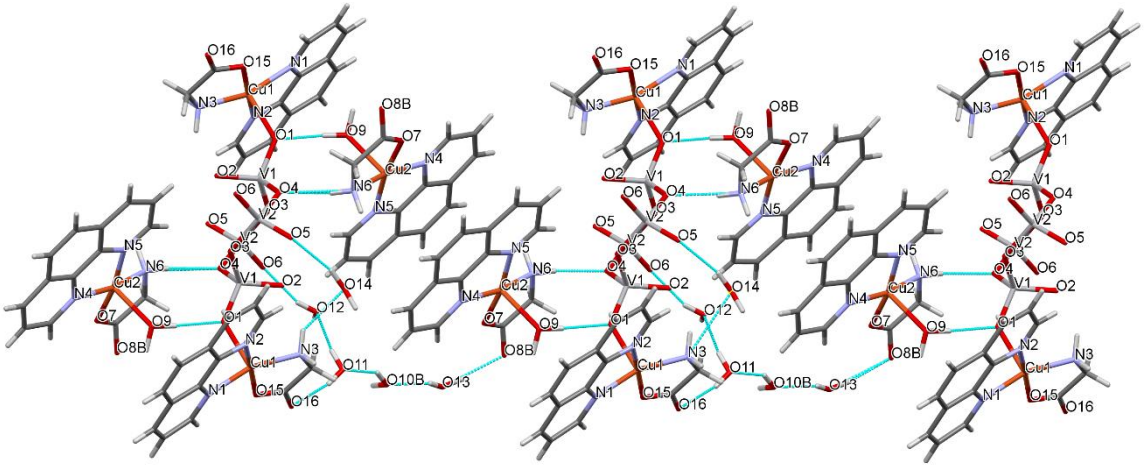

Figure 5. Capped stick representation of the hydrogen bond network communicating the cyclotetravandates in the [1,0,0] direction.

Table 2. Representative distances of **Compound 1**.

Atom-Atom	Length/Å	Theoretical/Å
Cu(1)-O(15)	1.9441(18)	1.9343
Cu(1)-N(2)	2.0127(19)	2.0304
Cu(1)-O(1)	2.2371(17)	2.2260
Cu(1)-N(1)	2.022(2)	2.0431
Cu(1)-N(3)	1.991(2)	2.0271
Cu(2)-N(5)	2.0178(19)	2.0212
Cu(2)-N(4)	1.9990(18)	2.0341
Cu(2)-O(7)	1.931(2)	1.9483
Cu(2)-N(6)	1.990(2)	2.0111
Cu(2)-O(9)	2.270(2)	2.3667
V(1)-O(4)	1.8067(16)	1.7929
V(1)-O(2)	1.8002(17)	1.7922
V(1)-O(1)	1.6665(15)	1.6507
V(1)-O(3)	1.6266(19)	1.6064
V(2)-O(4)	1.8166(15)	1.8268
V(2)-O(2)	1.8055(17)	1.8088
V(2)-O(5)	1.634(2)	1.6184
V(2)-O(6)	1.6448(19)	1.6109

Table 3. Hydrogen bond distances and angles for **Compound 1** [Å and °].

D—H···*A*	*D*—H	H···*A*	*D*···*A*	*D*—H···*A*
O9—H9*B*···O1	0.85	1.93	2.778 (3)	177
N3—H3*A*···O3	0.89	2.30	2.986 (3)	134
N3—H3*A*···O13*A*	0.89	2.31	3.050 (6)	140
N3—H3*B*···O14	0.89	2.24	3.056 (4)	153
N3—H3*B*···O13*B*	0.89	2.58	2.99 (2)	109
N6—H6*A*···O14^{i}	0.89	2.44	3.281 (4)	158
N6—H6*B*···O4	0.89	2.09	2.979 (3)	172
O9—H9*A*···O15^{ii}	0.86	2.34	3.028 (3)	137
O9—H9*A*···O16^{ii}	0.86	2.15	2.977 (3)	161
O9—H9*B*···O1	0.85	1.93	2.778 (3)	177
O11—H11*A*···O12^{iii}	0.97	1.89	2.808 (4)	157
O11—H11*B*···O16	0.94	1.90	2.813 (3)	164
O12—H12*A*···O6^{ii}	0.85	2.04	2.876 (3)	166
O12—H12*B*···O6^{iv}	0.85	1.99	2.833 (3)	176
O14—H14*A*···O8*A*^{ii}	0.85	1.84	2.602 (9)	149
O14—H14*A*···O8*B*^{ii}	0.85	1.84	2.670 (19)	167
O14—H14*B*···O10*A*^{v}	0.85	1.95	2.705 (11)	147
O14—H14*B*···O10*B*^{v}	0.85	1.92	2.663 (15)	145
O10*A*—H10*B*···O5^{vi}	0.85	1.97	2.781 (8)	160
O10*B*—H10C···O11^{vii}	0.85	2.03	2.761 (19)	144
O10*B*—H10*D*···O5^{vi}	0.85	1.92	2.755 (16)	166
O13*A*—H13*A*···O3	0.85	2.50	2.982 (4)	117
O13*A*—H13*A*···O5^{vi}	0.85	2.35	3.094 (5)	147
O13*A*—H13*B*···O14^{v}	0.85	1.96	2.751 (5)	155

Symmetry codes: (i) −x+2, −y+1, −z+1; (ii) x+1, y+1, z; (iii) −x+2, −y, −z+1; (iv) x−1, y−1, z; (v) −x+2, −y+1, −z+2; (vi) x−1, y, z; (vii) x−1, y, z.

3.2. Experimental IR and RAMAN Spectra

The infrared spectrum of **Compound 1** is shown in the section of theoretical IR. The spectrum shows a complex set of bands with peaks at 949 cm^{-1} and 924 cm^{-1}, which originated in the υs(VO-term) slightly coupled with Cu atom. The bands at 900, 876, 858 cm^{-1}, are attributed to the υa(VO-term). These 5 bands make a comb-like signature because each VO vibrates differently, since the neighbor oxygen atoms surrounding the vanadium ions are involved in different types of bonds [27,56]. Moreover, the bridging V-O-V bonds vibrate in the ~800 and 600 cm^{-1} region as symmetric and antisymmetric stretching modes. The bands at 764, 724, and 635 cm^{-1} are attributed to (VO-bridging). The bands at 738 and 432 cm^{-1} are typical vibrations of coordinated phenantroline. However, the last one could be due to Cu-N or Cu-O vibrations of the coordinated aminoacidate ions that could be in the same range.

The experimental Raman spectrum of **Compound 1** is shown in the section of theoretical Raman. The band at 950 cm^{-1} is due to the υs(VO-term), and the band at 710 cm^{-1} is attributed to the υs(VO-bridging) breathing modes. Finally, the one at 433 cm^{-1} could be assigned to the υs (Cu-N, Cu-O) of the coordinated aminoacidate or Cu-N of the coordinated phenantroline [57].

3.3. ^{51}V Nuclear Magnetic Resonance Spectroscopy

The ^{51}V NMR spectrum of **Compound 1** was measured in PBS/D_2O at 25 °C, showing the classic ^{51}V resonance signal assigned to cyclotetravanadate at −571 ppm. However, a new signal at −558 ppm, which is consistent with the anion $H_2VO_4^-$, was observed [58]. This suggests that the compound has been fragmented while redissolving it, generating an equilibrium between units of [Cu(phen)(Gly)(H_2O)]+ neutralized by $H_2VO_4^-$ anions, [Cu(phen)(Gly)(H_2O)]H_2VO_4, and the intact molecule. The $H_2VO_4^-$ ions could act as a monodentate or bidentate ligand, analogous to phosphate ions [59]. The spectrum is shown in Figure 6.

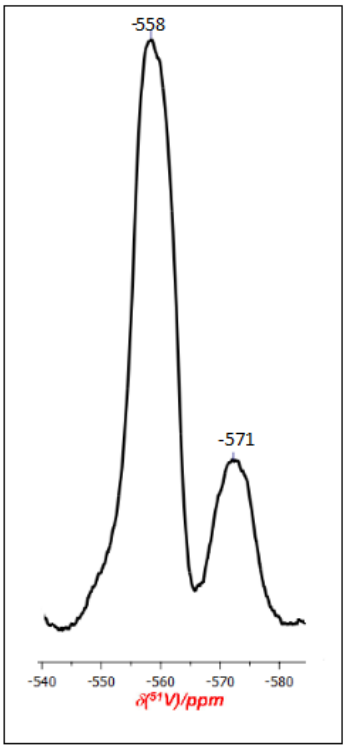

Figure 6. Vanadium-51 Nuclear Magnetic Resonace spectrum of **Compound 1** in phosphate-buffered saline (PBS)/D_2O.

3.4. Visible Spectroscopy

The UV-Vis spectrum of **Compound 1** is presented in Figure S4; the sample was made at a concentration of 0.35 mM, and it was dissolved in a phosphate-buffered saline (PBS) solution at pH 7.4. The sample showed an absorption band at 644 nm, with an absorbance of 0.083. Therefore, the molar extinction coefficient is $\varepsilon = 69\ Lmol^{-1}cm^{-1}$ per Cu atom. These values can be observed in the spectral window from 400 to 800 nm, which is typical of d–d transitions of Cu (II) complexes [60,61].

3.5. Cyclic Voltammetry

Cyclic voltammetry of the individual precursor salts NH_4VO_3 and $CuCl_2$, at a 1.0 mM concentration, was performed to assign redox peaks of **Compound 1**. This did not show any peaks that could be attributed to vanadium redox processes as compared to the voltammetry results reported by Çakir and Biçer [62], as seen in Figure S5. On the other hand, the $CuCl_2$ in solution shows an irreversible reduction peak at 0.17 V that can be related to the reduction of Cu (II) to Cu (0) [63], as seen in Figure S6. Glycine and 1,10-phenantroline were not electroactive within the same potential window. However, the cyclic voltammetry of **Compound 1** shows the redox quasi-reversible couple at −0.23 V and 0.050 V for the Cu (II)/Cu(I) redox pair [15] and consequently its formal potential is $E_{1/2} = -0.085$ V (see Figure 7). The voltammogram also showed the irreversible reduction peak from copper in solution at 0.17 V. After the addition of DNA, peaks from the redox Cu (II)/Cu(I) couple undergo a notorious decrease in current intensity, attributed to a decrease in mass transfer coefficient due to **Compound 1** being bonded to DNA [64,65], evidencing a strong interaction between them. Moreover, a slight shift towards a more positive reduction potential from −0.23 V to −0.22 V is observed for the reduction peak and also for the oxidation peak, which in DNA presence is at 0.038 V. Furthermore, a slight shift towards more negative potentials for the Cu (II)/Cu(I) redox pair formal potential, $E_{1/2} = -0.095$ V, is now observed. The positive potential shift on the reductive peak has been reported as evidence for DNA intercalation [66]. In contrast, the negative potential shift on $E_{1/2}$ has been reported as evidence for a molecule's electrostatic binding to the negatively charged deoxyribose-phosphate backbone of DNA [67]. Therefore, the DNA interactions shown by **Compound 1** are both intercalation and electrostatic binding.

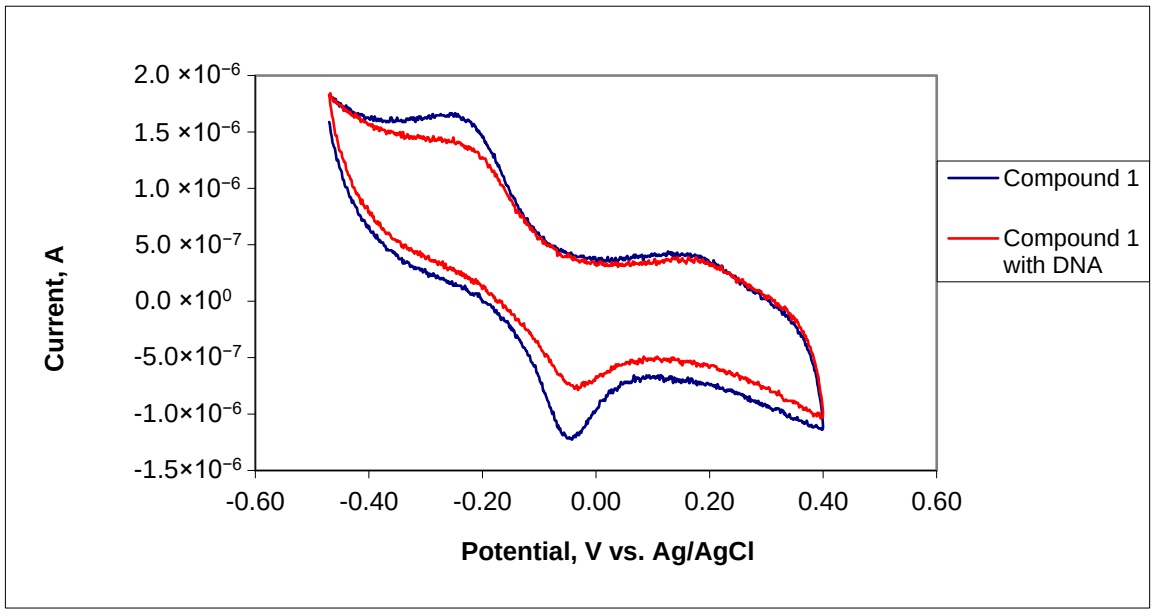

Figure 7. Cyclic voltammetry of **Compound 1** before and after DNA addition in phosphate buffer solution at pH 7.4, scan rate 0.05 V/s.

3.6. Theoretical Results

The presence of two types of copper atoms in **Compound 1** could suggest possible spin–spin interactions and a slight antiferromagnetic behavior. However, pathways using hydrogen bonds or π–π interactions could be responsible for interesting magnetic behavior. Thus, the presence of different spin states was investigated.

Our results show that the triplet state is more stable than the singlet and pentet states through single-point calculations and interaction energies with the counterpoise corrections, as can be seen in Table 4. The optimized molecular structure of **Compound 1** is obtained in its most stable state as a triplet. It is observed that the structure of spin-unrestricted M06-2X/Def2TZVP-LANL2TZ(f)/ECP = LANL2TZ(f) calculations is in reasonable agreement with the crystallographic values (see Table 2).

Table 4. Relative electronic energies (ΔE) and interaction energies (E_{int}) (in kcal mol^{-1}) for singlet, triplet, and pentet lowest electronic states of **Compound 1.**

Electronic State	ΔE (kcal mol^{-1})	E_{int} (kcal mol^{-1})
Singlet	15.3	−365.41
Triplet	0.00	−410.72
Pentet	0.10	−405.20

The molecular electrostatic potential (MEP) of **Compound 1** is shown in Figure 8. The isosurface shows the total electronic density mapped with the electrostatic potential using an isovalue of 0.004 a.u. The color code indicates that the red regions have a negative charge concentration, while the blue regions indicate a positive charge. Regions from yellow to green indicate intermediate values. From the isosurface in Figure 8, it can be seen that the zones with the highest charge density are located on the tetravanadate ion and the glycinate −COO group. In contrast, the zones with a positive charge are located in the regions of the phenanthroline molecules. The noncovalent interactions Cu···O(3)-V and Cu···O(9) are found in intermediate electron density zones.

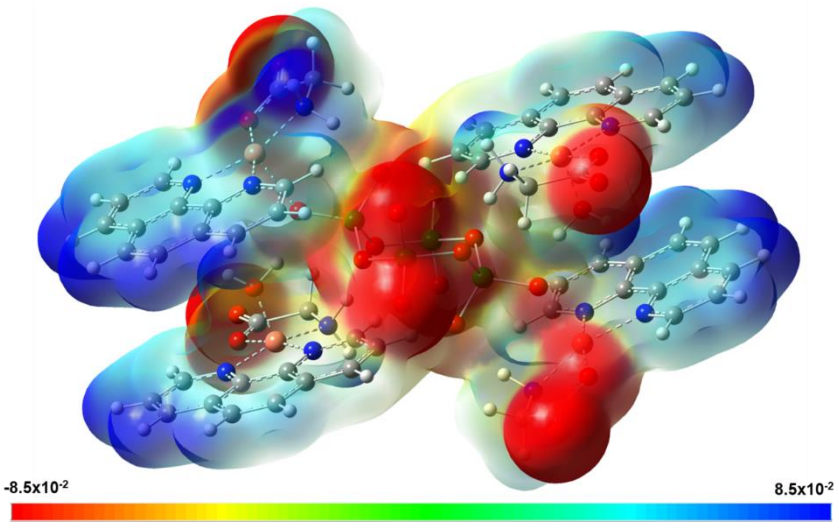

Figure 8. Molecular electrostatic potential (MEP) of **Compound 1** at the M06-2X/Def2TZVP-LANL2TZ(f) level of theory using the ECP = LANL2TZ(f) for V and Cu atoms in the polarizable conductor calculation model (CPCM) model and water solvent.

The population analysis used for evaluating the electron density of the molecular system can be based on the wave function through a natural population analysis (NPA). To obtain the natural charges for each atom, the NPA uses natural atomic orbitals (NAOs) and natural bond orbitals with maximum

electron density to localize the electrons in each atom, and therefore the dependence on the basis set is reduced. The most positive or most negative NPA charges are then indicators of the distribution of the electronic density in the molecule and the availability of attracting or donating electrons for the formation of covalent or noncovalent bonds. Consequently, the spin density derived from NPA calculations can be used to explain the electronic distribution in the molecular systems. Table 5 shows the natural charges of the atoms that participate in the interactions between the cyclotetravanadate ion and the organic counterions of Gly and phenanthroline coordinated with Cu.

Table 5. Selected relevant noncovalent interactions, Mayer bond order ($B_{Metal\cdots NoMetal}$), NPA spin density ($NPA_{Metal\cdots NoMetal}$) and free valence index of the metal atoms (FVI_{Metal}) in **Compound 1** at the M06-2X/Def2TZVP-LANL2TZ(f) level of theory using the ECP = LANL2TZ(f) for V and Cu in the CPCM model and water solvent.

Interactions	$B_{Metal\cdots NoMetal}$	$NPA_{Metal\cdots NoMetal}$	FVI_{Metal} (au)
Cu(1) ⋯ O(15)	0.341	1.073⋯ −0.806	0.076
Cu(1) ⋯ N(3)	0.282	1.073⋯ −0.974	0.076
Cu(1) ⋯ N(1)	0.244	1.073⋯ −0.548	0.076
Cu(1) ⋯ N(2)	0.243	1.073⋯ −0.546	0.076
Cu(1) ⋯ O(1)	0.201	1.073⋯ −0.635	0.076
V(1) ⋯ O(1)	1.661	1.884⋯ −0.636	2.15
Cu(2) ⋯ O(7)	0.332	1.091⋯ −0.800	0.085
Cu(2) ⋯ N(4)	0.241	1.091⋯ −0.552	0.085
Cu(2) ⋯ N(5)	0.238	1.091⋯ −0.551	0.085
Cu(2) ⋯ N(6)	0.295	1.091⋯ −0.945	0.085
Cu(2) ⋯ O(9)	0.178	1.091⋯ −0.935	0.085

From these results, it can be seen that the metal-ligand bond orders for the O(15) and N(3) atoms in Gly molecules, which are coordinated with Cu(1), are 0.341−0.282. In a similar and symmetrical way to the N(1) and N(2) atoms of phenantroline, the bond orders are 0.243−0.244. In addition, the bond order of the O(1) and O(9) atoms are 0.201 and 0.178, respectively, in an apical position on the squared pyramidal geometry. This is preserved both in the organic molecules coordinated with Cu(1) and in the molecules coordinated with Cu(2). On the other hand, in the values of the natural charges (NPA), it can be seen that N(3) and N(6) of Gly have a negative charge higher (−0.974 and −0.945, respectively) than N(1) and N(2) of phen (in a range from −0.546 to −0.552). Moreover, O(9) of H_2O (−0.935), which coordinates with Cu(2), has a more negative charge than the O(1) of cyclotetravanadate (−0.636) that coordinates with Cu(1). These results show that the contributions of the atoms of Cu, N, and O indicate significant noncovalent interactions to metal-ligand bonding and that it will be similar in both coordinated groups with Cu(1) and Cu(2).

The Hirshfeld surface of **Compound 1,** as shown in Figure 9A, presents information about the intermolecular interactions involved. The Hirshfeld surface was mapped with the normalized contact distance, d_{norm}. It is observed that the red spots on the Hirshfeld surface are due to close intermolecular interactions of mainly O⋯H, H⋯H, and H⋯O. Strong hydrogen bonds (i.e., 1.915, 2.056 and 2.17 Å) are observed between the cluster of water molecules with oxygens of ion $[V_4O_{12}]^{4-}$. These interactions are involved in the formation of the monodimensional supramolecular structure presented in Figure 3. The 2D representation of the intermolecular interactions is presented in the fingerprint plot in Figure 9B. In this case, d_i indicates the distance from the surface to the nearest nucleus inside the surface, and d_e is the distance from the surface to the nearest nucleus outside the surface. The contribution that is most significant is from interactions H⋯H (34.0%), which come from the result of noncovalent interactions of H atoms of phen and Gly with H atoms of phen, Gly, and H_2O external to Hirshfeld

surface. The contribution O···H (17.3%) is due to the interactions of hydrogen bonds between H atoms of H_2O with O atoms of the cyclotetravanadate anion, acting as an acceptor. In addition, the interactions of O atoms of Gly with H_2O adjacent contribute to O···H interactions. The interactions H···O (15.7%) are the result of noncovalent interactions of H atoms of phen with adjacent O atoms of Gly or H_2O in the crystal packing. Other interactions with minor contributions are C···C (11.0%), C···H (7.2%), and H···C (6.0%).

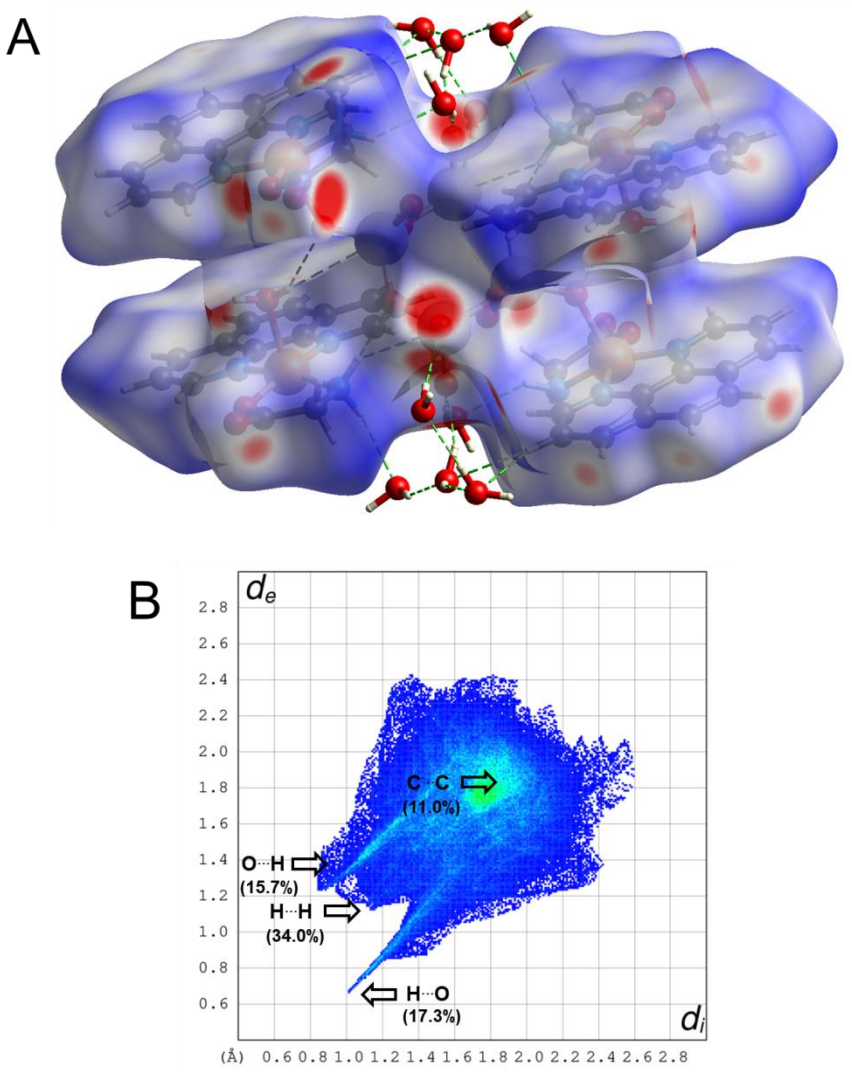

Figure 9. (**A**) Hirshfeld surface mapped with d_{norm} parameter. (**B**) Fingerprint plot of noncovalent interactions.

The theoretical IR and Raman spectra of **Compound 1** containing cyclotetravanadate clusters exhibit some characteristics signals in the 1000–400 cm^{-1} region, depending not only on the nature of the counterions or the formation of hydrogen bonds, but also on that of the coordination of the cyclotetravanadate moiety. Therefore, we performed a simulation of theoretical IR and Raman spectra based on the DFT of **Compound 1** in order to have a theoretical basis for the right assignment of the V=O and V-O-V vibration modes in both spectroscopies.

In Figure 10, the IR spectrum of **Compound 1** is shown. The main bands are assigned to the bending (C-H) of phen at 553 cm^{-1}, bridging (V-O) at 578–595 cm^{-1}, and 747–760 cm^{-1}. Moreover, in this region, bridging modes (V-O) coupled with bending modes (C-H) of phen and Gly counterions are observed. In the region of 907–987 cm^{-1}, the terminal stretching modes (V-O) are found.

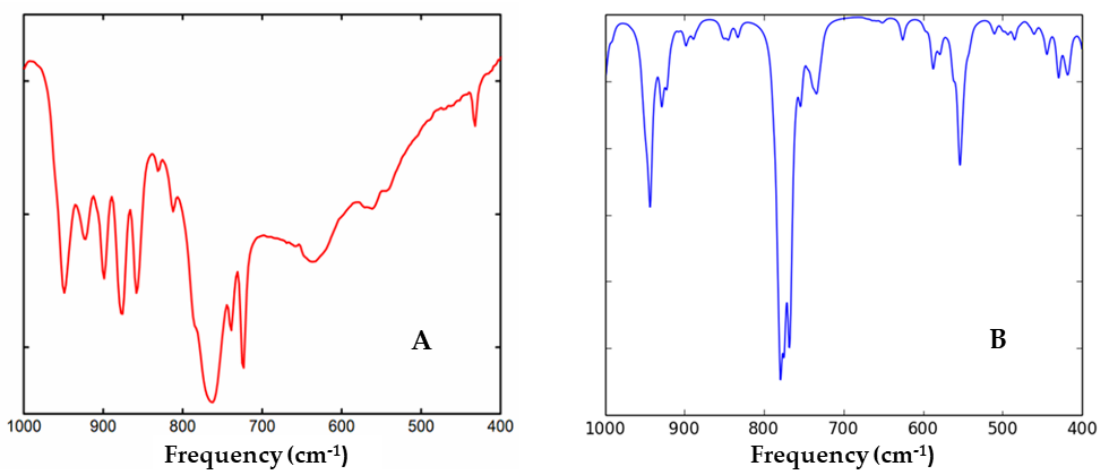

Figure 10. Experimental (**A**) and theoretical (**B**) IR spectrum of **Compound 1** calculated at the M06-2X/Def2TZVP-LANL2TZ(f) level of theory using the ECP = LANL2TZ(f) for V and Cu in the CPCM model and water solvent.

Figure 11 shows the experimental and theoretical Raman spectrum of **Compound 1**. In this case, the main absorption bands are assigned to the bending mode (C-H) of phen at 576 cm^{-1}, the bending mode (C-H) of Gly at 712 cm^{-1}, and the cyclotetravanadate bridging modes (V-O) in the region of 760–782 cm^{-1}, slightly coupled with bending modes (CH) of phen and Gly. At 813 cm^{-1}, a well-defined band of cyclotetravanadate bridging (V-O) is observed. In the region 908–990 cm^{-1}, the stretching terminal modes (V-O) are clearly observed.

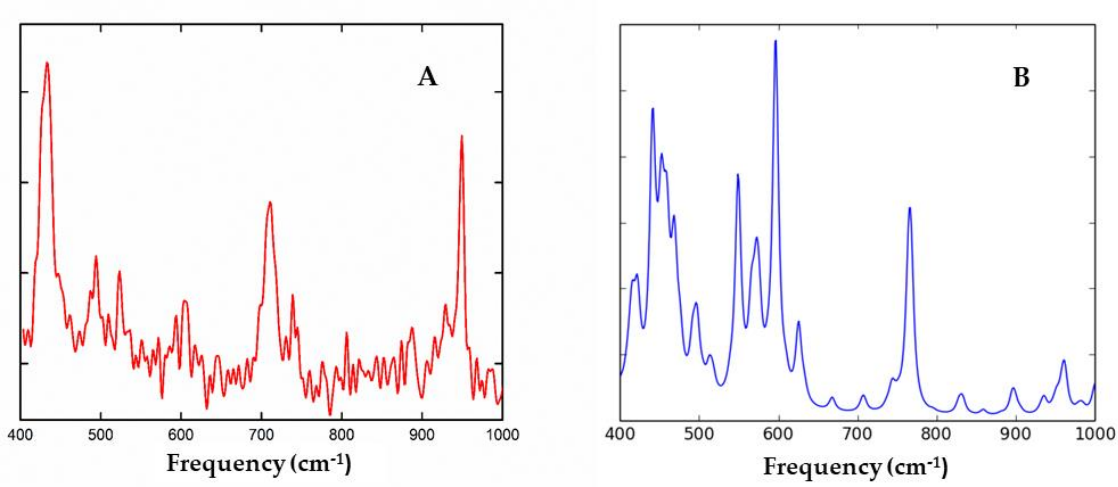

Figure 11. Experimental (**A**) and theoretical Raman spectrum (**B**) of **Compound 1** calculated at the M06-2X/Def2TZVP-LANL2TZ(f) level of theory using the ECP = LANL2TZ(f) for V and Cu in the CPCM model and water solvent.

4. Discussion

Over the past two decades, there have been extensive studies about DNA interaction with transition metal complexes aimed at developing spectroscopic or electrochemical DNA probes, chemical nucleases, and biomedical reagents. Transition metal complexes can easily interact with DNA through intercalation, groove binding, and external electrostatic binding [3]. Many useful applications of these complexes require that the complex bind to DNA through an intercalative mode with the ligand intercalating into the adjacent base pairs of the DNA molecule. This behavior is frequently found in copper (II) complexes. The square pyramidal structure characteristic of this type of compounds interacts with DNA, and this renders them as alternatives to platinum-based

anticancer drugs with the advantage that copper is better tolerated and can be more easily handled than other transition metals. Much attention has been paid to complexes containing symmetric aromatic ligands, such as 1,10-phenanthroline and 2,2′-bipyridyl, as well as the way they interact with DNA [3,68–70]. This interest began when Kwik et al. (1980) first synthesized and characterized a series of ternary complexes, including [Cu(phen)L]·nH_2O, [Cu(bipy)L]·nH_2O, [Cu(phen)LX]·nH_2O and [Cu(bipy)LX]·nH_2O [71]. Since then, several studies have shown that the geometry exhibited by the metal center, coupled with planar bidentate ligands, contains an optimal structure to interact with many biological molecules and has antitumoral and antiviral properties. Copper (II) complexes containing 1,10-phenanthroline can also function as chemical nucleases. Sigman et al. (1979) demonstrated that $[Cu(phen)_2]^+$ complexes inhibit DNA or RNA polymerase activities and can induce the scission of DNA strands in the presence of H_2O_2 or thiols [72]. The mechanism occurs by a Cu (II)/Cu (I) redox reaction that catalyzes the formation of reactive oxygen species (ROS). The structure of this type of complexes consists of a five-coordinate copper (II) center displaying a distorted square pyramidal geometry. These types of complexes exhibit an efficient DNA cleavage activity at micromolar concentrations in the presence of ascorbate with hydroxyl radicals as the active species [73]. The compound is a different presentation of the well-known compound crystallized initially as nitrate salt. A similar compound was crystallized containing chloride ion instead of water in the apical position of the squared pyramidal geometry. The molecular structure of **Compound 1** is highly reminiscent of Casiopeínas® (CAS), which are a series of copper-based drugs developed by Ruiz-Azuara and coworkers [74,75]. CAS are mixed chelate copper (II) complexes with a general condensed formula [Cu(N–N)(A–A)]NO_3, where N–N represents neutral diimine donors, either phenantroline or bipyridine derivatives, and A–A stands for uninegative N–O or O–O donors, either aminoacidates or acetylacetonate [76,77]. As shown above, DNA is the primary target molecule for most anticancer and antiviral therapies. Therefore, the goal has been to develop planar organic compounds that can bind to DNA by the intercalation of aromatic heterocyclic rings like the phenanthroline/bipyridine between the DNA base pairs. Copper complexes incorporating Schiff bases, amino acids, peptides, azoles, terpyridines, or polypyridyls as ligands as well as dinuclear copper complexes and copper complexes incorporating natural products or bioactive ligands showing metallonuclease activity have been reviewed [78]. Recently, a series of ternary copper (II)-L-dipeptide-neocuproine complexes have shown cytotoxicity against cancer cells, including MDA-MB-231, the triple-negative breast cancer [79].

In a recent contribution from our group, the molecular docking information obtained with two similar structures suggests that the heterobimetallic compounds provide a potential alternative to platinum anticancer drugs, bringing two antitumor metal agents together in a useful geometry [32]. The case of **Compound 1** in a solution will release the compound named Casiopeina® VII-Gly, which is structurally similar to Casiopenia® II-Gly, one of the most studied compounds of this type that has shown promising results in preclinical studies and is currently in phase 1 clinical trials in Mexico [80]. Moreover, the cyclic voltammetry experiments suggest the interaction of **Compound 1** with DNA due to electrostatic attraction and intercalation. Not only does the compound have the structural characteristics of Cu-based metallodrugs, but it also has the vanadium moiety that allows for a possible bimodal way of action, as pointed out by recent reports of vanadium compounds useful in pancreatic cancer and malignant melanoma [81,82].

5. Conclusions

A heterobimetallic V/Cu complex with the cyclotetravanadate anion acting as a bridge was synthesized and characterized by elemental analysis; visible, FTIR, and Raman spectroscopies; ^{51}V NMR analyses; cyclic voltammetry; as well as X-ray diffraction. The complex was also characterized by theoretical methods using DFT methodology. The theoretical calculation was of great value to understand the experimental results. The IR and Raman theoretical spectra calculations are less complicated than the experimentally measured spectra, mainly due to the complex set of hydrogen bonds in the solid state. However, the calculations allowed for a more detailed assignation of the most

relevant vibrational motions of the compounds. Cyclic voltammetry suggests interaction with DNA through intercalation and electrostatic interactions. The complex, also known as Casiopeína VII-gly, has shown nuclease activity in a variety of cancer cells. In this case, the compound was crystallized as the cyclotetravanadate, with the peculiarity of $[V_4O_{12}]^{4-}$ being bound to two copper ions and being neutralized with another two $[Cu(phen)(Gly)(H_2O)]^+$ moieties. The compound is structurally interesting because of two types of copper atoms and 24 hydrogen bonds, which are responsible for a 3D supramolecular structure. It also shows an interesting monodimensional array also mediated by hydrogen bonds and π–π interactions. These exciting features deserve further studies of magnetic behavior, which are now in progress. Another interesting characteristic is that all the components have revealed to be able to interact with DNA molecules and act in vivo as metallonucleases. They also represent a new member of a recent family of heterobimetallic potential metallodrugs [83].

On the other hand, vanadate and oligovanadates also have the potential to act as anticancer drugs, as shown recently for pancreatic cancer and malignant melanoma [84–86]. In our case, the cyclotetravanadate ion may serve as a source of $(H_2VO_4)^-$, $(V_4O_{12})^{4-}$, and $(V_{10}O_{28})^{6-}$ ions, depending on the concentration and pH of the cell compartments where they could be released. Thus, we provide a new potential pro-metallodrug whose components may act in conjunction, releasing all their constituents in vivo and which may be tested in a variety of cancer models.

Supplementary Materials: The following are available online at http://www.mdpi.com/2073-4352/10/6/492/s1, Figure S1: Packing of the unit cell of **Compound 1**. Figure S2: Ball and stick representation of the Cyclo-tetravanadate dicopper moiety of **Compound 1**. Figure S3: Copper-Copper distance Cu1—Cu2. Figure S4: The visible spectrum of **Compound 1** in PBS. Figure S5: Cyclic voltammetry of NH_4VO_3 in phosphate buffer solution at pH 7.4, scan rate 0.5 V/s. Figure S6: Cyclic voltammetry of $CuCl_2$ in phosphate buffer solution at pH 7.4, scan rate 0.1 V/s. TABLE S1: Fractional atomic coordinates and isotropic or equivalent isotropic displacement parameters (Å2) for **Compound 1**. Table S2: Geometric parameters (Å, °) for **Compound 1**.

Author Contributions: B.M.-V., N.D.C.-M., and E.S.-L. carried out the experimental work (synthesis, crystallization, and experimental characterization). M.C.-L. designed and performed the cyclic voltammetry experiments. A.M. carried out the X-ray diffraction experiment and wrote the X-ray diffraction results. F.J.M.-B. and M.E.C. carried out the theoretical characterization. E.G.-V. and B.L.S.-G. wrote and revised the manuscript. B.M.-V., N.D.C.-M., and E.G.V. conceived and designed this study. All authors contributed extensively to the work presented in this paper. All authors have read and agreed to the published version of the manuscript.

Funding: This research was funded by projects 100108444-VIEP2019 and 100256333-VIEP2019, as well as by the PRODEP Academic Group BUAP-CA-263 (SEP, Mexico).

Acknowledgments: B.M.V., N.D.C.M., and E.S.L. wish to thank CONACyT (Mexico) for the fellowship support numbers 390894, 593307, and 293256. M.E.C. and F.J.M. wish to thank Laboratorio Nacional de Supercómputo del Sureste de México (LNS-BUAP) and CONACyT network of national laboratories for the computer resources and support provided. We thank PRODEP Academic Group BUAP-CA-263 (SEP, Mexico). We also thank Enrique Sánchez Mora and Dra. Laura Serrano de la Rosa for the FT-Raman measurements carried out at Laboratorio Central del Instituto de Física Luis Rivera Terrazas (IFUAP). Amalia García and Antonio Dieguez, University of Granada, Spain, contributed to the X-ray diffraction refinement. Jorge Jiménez Cisneros and M.Sc. Ana Laura Manzano Covarrubias were involved in the CV experiments and DNA extraction, respectively. We thank the support provided by VIEP-BUAP through Yadira Rosas Bravo for the observations and comments to improve this manuscript.

Conflicts of Interest: There are no conflicts of interest to declare.

References

1. Rosenberg, B.; Van Camp, L.; Krigas, T. Inhibition of cell division in Escherichia coli by electrolysis products from a platinum electrode. *Nature* **1965**, *205*, 698–699. [CrossRef]
2. Manzano, C.; Pellei, M.; Tisato, F.; Santini, C. Copper complex as anticancer agents. *Anti-Cancer Agents Med. Chem.* **2009**, *9*, 185–211. [CrossRef] [PubMed]
3. Rabik, C.A.; Dolan, M.E. Molecular mechanisms of resistance and toxicity associated with platinating agents. *Cancer Treat. Rev.* **2007**, *33*, 9–23. [CrossRef] [PubMed]

4. Correia, I.; Roy, S.; Matos, C.P.; Borovic, S.; Butenko, N.; Cavaco, I.; Marques, F.; Lorenzo, J.; Rodríguez, A.; Moreno, V.; et al. Vanadium(IV) and copper(II) complexes of salicylaldimines and aromatic heterocycles: Cytotoxicity, DNA binding, and DNA cleavage properties. *J. Inorg. Biochem.* **2015**, *147*, 134–146. [CrossRef] [PubMed]
5. Denoyer, D.; Clatworthy, S.A.S.; Cater, M.A. Copper Complexes in Cancer Therapy. *Met. Ions Life Sci.* **2018**, *18*, 469–506.
6. Aureliano Santini, C.; Pellei, M.; Gandin, V.; Porchia, M.; Tisato, F.; Manzano, C. Advances in Copper Complexes as Anticancer Agents. *Chem. Rev.* **2014**, 815–862.
7. Li, H.; Wang, J.; Wu, C.; Wang, L.; Chen, Z.S.; Cui, W. The combination of disulfiram and copper for cancer treatment. *Drug Discov. Today.* **2020**. [CrossRef]
8. Ezhilarasan, D.; Arumugham, M.N. Synthesis, characterization DNA binding and biological activity of Copper(II) complexes with mixed ligands. *J. Chem. Biol. Phys. Sci.* **2017**, *7*, 896–905.
9. Kucková, L.; Jomová, K.; Švorcová, A.; Valko, M.; Segľa, P.; Moncoľ, J.; Kožíšek, J. Synthesis, crystal structure, spectroscopic properties and potential biological activities of salicylate-neocuproine ternary copper (II) complexes. *Molecules* **2015**, *20*, 2115–2137. [CrossRef]
10. Pages, B.J.; Ang, D.L.; Wright, E.P.; Aldrich-Wright, J.R. Metal complex interactions with DNA. *Dalton Trans.* **2015**, *44*, 3505–3526. [CrossRef]
11. Ng, C.H.; Kong, S.M.; Lian, Y.; Jamil, M.; Sukram, N.; Ahmad, M.; Khoo, A.S.B. Selective anticancer copper(II)-mixed ligand complexes: Targeting of ROS and proteasomes. *Metallomics* **2014**, *6*, 892–906. [CrossRef]
12. Tovar, A.; Ruiz-Ramirez, L.; Campero, A.; Romerosa, A.; Moreno-Esparza, R.; Rosales-Hoz, H. Structural and reactivity studies on 4,4-dimethyl-2,2-bipyridine acetylacetonate copper(II) nitrate (CASIOPEINA III-ia) with methionine, by UV–visible and EPR techniques. *J. Inorg. Biochem.* **2004**, *98*, 1045–1053. [CrossRef]
13. Erxleben, A. Interactions of copper complexes with nucleic acids. *Coord. Chem. Rev.* **2018**, *360*, 92–121. [CrossRef]
14. Baskaran, S.; Krishnan, M.M.; Arumugham, M.N.; Kumar, R.J. DFT analysis and DNA binding, cleavage of copper(II) complexes. *Mol. Liq.* **2016**, *221*, 1045–1053. [CrossRef]
15. Bravo-Gómez, M.E.; García-Ramos, J.C.; Gracia-Mora, I.; Ruiz-Azuara, L. Antiproliferative activity and QSAR study of copper (II) mixed chelate [Cu (N–N)(acetylacetonate)] NO3 and [Cu (N–N)(glycinato)] NO3 complexes,(Casiopeínas®). *J. Inorg. Biochem.* **2009**, *103*, 299–309. [CrossRef] [PubMed]
16. Valdez-Camacho, J.R.; Pérez-Salgado, Y.; Espinoza-Guillén, A.; Gómez-Vidales, V.; Tavira-Montalvan, C.A.; Meneses-Acosta, A.; Leyva, M.A.; Vázquez-Ríos, M.G.; Juaristi, E.; Höpfl, H.; et al. Synthesis, structural characterization and antiproliferative activity on MCF- T 7 and A549 tumor cell lines of [Cu(N-N)(β3-aminoacidate)]NO_3 complexes (Casiopeínas®). *Inorg. Chim. Acta* **2020**, *506*, 119542. [CrossRef]
17. Mejia, C.; Ortega-Rosales, S.; Ruiz-Azuara, L. Mechanism of Action of Anticancer Metallodrugs. In *Biomedical Applications of Metals*; Chapter 10; Springer: Berlin/Heidelberg, Germany, 2018; pp. 213–234.
18. Treviño, S.; Díaz, A.; Sánchez-Lara, E.; Sanchez-Gaytan, B.L.; Perez-Aguilar, J.M.; González-Vergara, E. Vanadium in Biological Action: Chemical, Pharmacological Aspects, and Metabolic Implications in Diabetes Mellitus. *Biol. Trace Elem. Res.* **2019**, *188*, 68–98. [CrossRef]
19. Bishayee, A.; Waghray, A.; Patel, M.A.; Chatterjee, M. Vanadium in the detection, prevention and treatment of cancer: The in vivo evidence. *Cancer Lett.* **2010**, *294*, 1–12. [CrossRef]
20. Crans, D.; Yang, L.; Haase, A.; Yang, X. Metallo-Drugs: Development and Action of Anticancer Agents. *Met. Ions Life Sci. Book* **2018**, *18*, 251–280.
21. Crans, D.; Smee, J.; Gaidamauskas, E.; Yang, L. The Chemistry and Biochemistry of Vanadium and the Biological Activities Exerted by Vanadium Compounds. *Chem. Rev.* **2004**, *104*, 849–902. [CrossRef]
22. Kioseoglou, E.; Petanidis, S.; Gabriel, C.; Salifoglou, A. The chemistry and biology of vanadium compounds in cancer therapeutics. Coordination. *Coord. Chem. Rev.* **2015**, *301–302*, 87–105. [CrossRef]
23. Novotny, L.; Kombian, S.B. Vanadium: Possible use in cancer chemoprevention and therapy. *J. Cancer Res. Updates* **2014**, *3*, 97–102. [CrossRef]
24. Chatterjee, M.; Schwab, M. (Eds.) *Encyclopedia of Cancer*; Springer: Berlin/Heidelberg, Germany, 2011; pp. 3883–3885.
25. Shobha, C.; Thulasiram, B.; Aerva, R.; Nagababu, P. Recent Advances in Copper Intercalators as Anticancer Agents. *J. Fluoresc.* **2018**, *28*, 1195–1205. [CrossRef] [PubMed]

26. Rehder, D. The potentiality of vanadium in medicinal applications. *Future Med. Chem.* **2012**, *4*, 1823–1837. [CrossRef] [PubMed]
27. Xiao, D.; An, H.; Wang, E.; Sun, C.; Xu, L. Synthesis and structure of a novel one-dimensional vanadate constructed from tetravanadate clusters linked via copper–organic complex moieties: [{Cu(phen)(H_2O)}$_2$$V_4O_{12}$]. *J. Coord. Chem.* **2006**, *59*, 827–835. [CrossRef]
28. Kucsera, R.; Joniaková, D.; Zúrková, L. Thermal properties of [MII (phen)$_3$]$_2$$V_4O_{12}$ phen 22H_2O (M II = Co, Ni, Cu, phen = 1,10-phenanthroline). *J. Therm Anal Calorim.* **2004**, *78*, 263–272. [CrossRef]
29. Paredes-García, V.; Gaune, S.; Saldías, M.; Garland, M.T.; Baggio, R.; Vega, A.; El Fallah, M.S.; Escuer, A.; Fur, E.L.; Venegas-Yazigi, D.; et al. Solvatomorphs of dimeric transition metal complexes based on the V4O12 cyclic anion as building block: Crystalline packing and magnetic properties. *Inorg. Chim. Acta.* **2008**, *361*, 3681–3689. [CrossRef]
30. Wang, Q.; Yu, X.L.; You, W.S.; Zhao, Y.; Huang, C.Y.; Sun, Z.G. Two novel isomeric complexes supported by vanadates {V_4O_{12}}:[{Cu(dpa)$_2$}$_2$$V_4O_{12}$](dpa = 2,2′-dipyridylamine). *Inorg. Chem. Commun.* **2007**, *10*, 1465–1468. [CrossRef]
31. Joniaková, D.; Gyepes, R.; Rakovský, E.; Schwendt, P.; Marek, J.; Mička, Z. Structural variability of copper-1,10-phenanthroline–oxovanadate hybrid inorganic–organic compounds. *Polyhedron* **2006**, *25*, 2491–2502. [CrossRef]
32. Martínez-Valencia, B.; Corona-Motolinia, N.D.; Sánchez-Lara, E.; Noriega, L.; Sánchez-Gaytán, B.L.; Castro, M.E.; Meléndez-Bustamante, F.; González-Vergara, E. Cyclo-tetravanadate bridged copper complexes as potential double bullet pro-metallodrugs for cancer treatment. *J. Inorg. Biochem.* **2020**, 111081. [CrossRef]
33. Bray, F.; Ferlay, J.; Soerjomataram, I.; Siegel, R.L.; Torre, L.A.; Jemal, A. Global cancer statistics 2018: GLOBOCAN estimates of incidence and mortality worldwide for 36 cancers in 185 countries. *CA Cancer J. Clin.* **2018**, *68*, 394–424. [CrossRef]
34. Mjos, K.D.; Orving, C. Metallodrugs in Medicinal Inorganic Chemistry. *Chem. Rev.* **2014**, *114*, 4540–4563. [CrossRef] [PubMed]
35. Becco, L.; García-Ramos, J.C.; Azuara, L.R.; Gambino, D.; Garat, B. Analysis of the DNA interaction of copper compounds belonging to the Casiopeínas® antitumoral series. *Biol. Trace Elem. Res.* **2014**, *161*, 210–215. [CrossRef] [PubMed]
36. CrysAlis, P.R.O. Agilent Technologies Ltd.: Oxford, UK, 2014. Available online: https://www.agilent.com/cs/library/usermanuals/Public/CrysAlis_Pro_User_Manual.pdf (accessed on 4 June 2020).
37. Dolomanov, O.V.; Bourhis, L.J.; Gildea, R.J.; Howard Puschmann, J.A.K. OLEX2: A complete structure solution, refinement, and analysis program. *J. Appl. Crystallogr.* **2009**, *42*, 339–341. [CrossRef]
38. Sheldrick, G.M. Crystal Structure Refinement with SHELXL. *Acta Crystallogr. Sect. C Struct. Chem.* **2008**, *A64*, 112–122.
39. Macrae, C.F.; Sovago, I.; Cottrell, S.J.; Galek, P.T.; McCabe, P.; Pidcock, E.; Platings, M.; Shields, G.P.; Stevens, J.S.; Wood, P.A.; et al. Mercury 4.0: From visualization to analysis, design and prediction. *J. Appl. Cryst.* **2020**, *53*, 226–235. [CrossRef] [PubMed]
40. Parr, R.G.; Yang, W. *Density-Functional Theory of Atoms and Molecules. International Series of Monograph on Chemistry 16*; Oxford University Press: New York, NY, USA, 1989; ISBN 978-0-19–987872-7.
41. Boys, S.F.; Bernardi, F. Calculation of Small Molecular Interactions by Differences of Separate Total Energies—Some Procedures with Reduced Errors. *Mol. Phys.* **1970**, *19*, 553. [CrossRef]
42. Simon, S.; Duran, M.; Dannenberg, J.J. How does basis set superposition error change the potential surfaces for hydrogen bonded dimers? *J. Chem. Phys.* **1996**, *105*, 11024–11031. [CrossRef]
43. Zhao, Y.; Truhlar, D.G. The M06 suite of density functionals for main group thermochemistry, thermochemical kinetics, noncovalent interactions, excited states, and transition elements: Two new functionals and systematic testing of four M06-class functionals and 12 other functionals. *Theor. Chem. Acc.* **2008**, *120*, 215–241.
44. Weigend, F.; Ahlrichs, R. Balanced basis sets of split valence, triple zeta valence and quadruple zeta valence quality for H to Rn: Design and assessment of accuracy. *Phys. Chem. Chem. Phys.* **2005**, *7*, 3297–3305. [CrossRef]
45. Weigend, F. Accurate Coulomb-fitting basis sets for H to Rn. *Phys. Chem. Chem. Phys.* **2006**, *8*, 1057–1065. [CrossRef] [PubMed]
46. Roy, L.E.; Hay, P.J.; Martin, R.L.J. Revised Basis Sets for the LANL Effective Core Potentials. *J. Chem. Theory Comput.* **2008**, *4*, 1029–1031. [CrossRef] [PubMed]

47. Ehlers, A.; Böhme, M.S.; Dapprich, A.; Gobbi, A.; Höllwarth, V.; Jonas Köhler, K.; Stegmann, R.; Veldkamp, A.; Frenking, G. A set of f-polarization functions for pseudo-potential basis sets of the transition metals SC-Cu, Y-Ag and La-Au. *Chem. Phys. Lett.* **1993**, *208*, 111–114. [CrossRef]
48. Hay, P.J.; Wadt, W.R. Ab initio effective core potentials for molecular calculations. Potentials for the transition metal atoms Sc to Hg. *J. Chem. Phys.* **1985**, *82*, 299–310. [CrossRef]
49. Cossi, M.; Rega, N.; Scalmani, G.; Barone, V. Energies, Structures, and Electronic Properties of Molecules in Solution with the C-PCM Solvation Model. *J. Comput. Chem.* **2003**, *24*, 669–681. [CrossRef]
50. Foster, J.P.; Weinhold, F. Natural hybrid orbitals. *J. Am. Chem. Soc.* **1980**, *102*, 7211–7218. [CrossRef]
51. Reed, A.E.; Curtiss, L.A.; Weinhold, F. Intermolecular interactions from a natural bond orbital, donor-acceptor viewpoint. *Chem. Rev.* **1988**, *88*, 899–926. [CrossRef]
52. Frisch, M.J.; Trucks, G.W.; Schlegel, H.B.; Scuseria, G.E.; Robb, M.A.; Cheeseman, J.R. *Gaussian 16, Revision, B.01*; Gaussian, Inc.: Wallingford, CT, USA, 2016.
53. Dennington, R.D., II; Keith, T.A.; Millam, J.M. *Gauss View, Version 6.0.16*; Semichem, Inc.: Shawnee Mission, UK, 2016.
54. Turner, M.J.; MacKiinnon, J.J.; Wolff, S.K.; Grimwood, D.J.; Spackman, P.R.; Jayatilaka, D.; Spackman, M.A. *CRYSTAL EXPLORER*; University of Western Australia: Perth, Australia, 2017. Available online: https://crystalexplorer.scb.uwa.edu.au/ (accessed on 4 June 2020).
55. Addison, A.W.; Rao, T.N.; Reedijk, J.; Van Rijn, J.; Verschoor, G.C. Synthesis, structure, and spectroscopic properties of copper (II) compounds containing nitrogen–sulphur donor ligands; the crystal and molecular structure of aqua [1,7-bis (N-methylbenzimidazol-2′-yl)-2,6-dithiaheptane] copper (II) perchlorate. *J. Chem. Soc. Dalton Trans.* **1984**, *7*, 1349–1356. [CrossRef]
56. Sharma, R.P.; Ajnesh, S.; Venugopalan, P.; Dansby-Sparks, R.; Xue, Z.L.; Rossetti, S.; Ferretti, V. Stabilization of tetrameric metavanadate ion by tris (1,10-phenanthroline) cobalt(III): Synthesis, spectroscopic, and X-ray structural study of [Co (phen)$_3$]$_3$(V$_4$O$_{12}$)$_2$Cl 27H$_2$O. *J. Coord. Chem.* **2010**, *63*, 3016–3027. [CrossRef]
57. Zhang, K.; Liang, D.; Wang, M.H. Bis[tris(2,2′-bipyridyl-κ2N,N′)cobalt(II)] cyclo-tetravanadate undecahydrate. *Acta Crystallogr. Sect. C Cryst. Struct. Commun.* **2013**, *69*, 138–141. [CrossRef]
58. Rehder, D. *Bioinorganic Vanadium Chemistry*; John Wiley & Sons Ltd.: Chichesterm, UK, 2008; Volume 18, p. 59.
59. Sastry, M.S.; Kesevadas, T.; Rao, G.S.; Sastry, M.D. Phosphate coordination in copper(II) complexes. *Proc. Indian Acad. Sci. (Chem. Sci.)* **1984**, *93*, 843–848.
60. Zhang, W.; Lu, X.; Wang, G.; Cheng, Y.; Zhang, B. Methyl-substituted enhancement of antitumor activity in square-planar metal complex and analysis of DE, DG, CV, UV-vis, and luminescence. *New J. Chem.* **2015**, *39*, 4869–4875. [CrossRef]
61. Sciortino, G.; Maréchal, J.D.; Fábián, I.; Lihi, N.; Garribba, E. Quantitative prediction of electronic absorption spectra of copper (II)–bioligand systems: Validation and applications. *J. Inorg. Biochem.* **2020**, *204*, 110953. [CrossRef]
62. Cakir, S.; Bicer, E. Voltammetric and Spectroscopic Studies of Vanadium (V)-Nicotinamide Interactions at Physiological pH. *Turk. J. Chem.* **2007**, *31*, 223–231.
63. Haque, F.; Rahman, M.S.; Ahmed, E.; Bakshi, P.K.; Shaik, A.A. A Cyclic Voltammetry Study of the Redox Reaction of Cu(II) in the presence of Ascorbic Acid in Different pH Media. Dhaka Univ. *J. Sci.* **2013**, *61*, 161–166.
64. Lu, X.; Zhu, K.; Zhang, M.; Liu, H.; Kang, J. Voltammetric studies of the interaction of transition-metal complexes with DNA. *J. Biochem. Biophys. Methods* **2002**, *52*, 189–200. [CrossRef]
65. Mohamed, M.I.; Shaban, Y.S.; Abd El-Motaled, M.R.; Mohamed, A.A.; Gaber, A.M.M.; Samir, A.E.-S.; Salih, A.-J. Ternary Copper (II) and Nickel (II) chelates of 2,2′-Bipyridyl and glycine: X-ray structures, kinetics, DNA binding, and cleavage activities. *J. Mol. Struct.* **2019**, *1198*, 126911.
66. Janjua, N.K.; Akhter, Z.; Jabeen, F.; Iftikar, B. Cyclic Voltammetric Investigation of Interactions between Bisnitroaromatic Compounds and ds. DNA. *J. Korean Chem. Soc.* **2014**, *58*, 153–159. [CrossRef]
67. Ni, Y.; Lin, D.; Kokot, S. Synchronous fluorescence, UV-visible spectrophotometric, and voltammetric studies of the competitive interaction of bis(1,10-phenanthroline)copper(II) complex and neutral red with DNA. *Anal. Biochem.* **2006**, *352*, 231–242. [CrossRef]

68. Dhakshanamoorthy, S.; Krishnan, M.M.; Arumugham, M.N. Synthesis, Characterisation, DNA Binding/Cleavage, Anticancer and Antimicrobial Activity of Ternary Copper(II) Complexes. *Asian J. Res. Chem.* **2017**, *10*, 312–318. [CrossRef]
69. Zou, X.H.; Ye, B.H.; Li, H.; Zhang, Q.L.; Chao, H.; Liu, J.G.; Ji, L.N.; Li, X.Y. The design of new molecular "light switches" for DNA. *J. Biol. Inorg. Chem.* **2001**, *6*, 143–150. [CrossRef]
70. Chao, H.; Mei, W.J.; Huang, Q.W.; Ji, L.N. NA binding studies of ruthenium(II) complexes containing asymmetric tridentate ligands. *J. Inorg. Biochem.* **2002**, *92*, 165–170. [CrossRef]
71. Kwik, W.L.; Ang, K.P.; Chen, G. Complexes of (2,2′-bipyridyl) copper(II) and (1,10-phenanthroline) copper(II) with some amino acids. *J. Inorg. Nucl. Chem.* **1980**, *42*, 303–313. [CrossRef]
72. Sigman, D.S.; Graham, D.R.; Aurora, V.D.; Stern, A.M. Oxygen-dependent cleavage of DNA by the 1,10-phenanthroline. cuprous complex. Inhibition of Escherichia coli DNA polymerase I. *J. Biol. Chem.* **1979**, *254*, 12269–12272.
73. Zhang, S.; Chun, X.; Chen, Y.; Zhou, J. Synthesis, Crystal Structure and DNA Cleavage Activity of a Ternary Copper(II) Complex of Dipyrido[3,2-d:2′,3′-f]-quinoxaline and Glycine. *Chin. J. Chem.* **2011**, *29*, 65–71. [CrossRef]
74. Alemon-Medina, R.; Brena-Valle, M.; Muñoz-Sánchez, J.L.; Gracia-Mora, M.I.; Ruiz-Azuara, L. Induction of oxidative damage by copper-based antineoplastic drugs (Casiopeínas). *Cancer Chemother. Pharmacol.* **2007**, *60*, 219–228. [CrossRef]
75. Ruiz-Azuara, L. Preparation of new mixed copper aminoacidate complexes from phenylated phenantrolines to be used as "anticancerigenic agents.". U.S. Patent 07 628.628, Re 35,458, 1992.
76. Rodríguez-Enríquez, S.; Vital-González, P.A.; Flores-Rodríguez, F.L.; Marín-Hernández, A.; Ruiz-Azuara, L.; Moreno-Sánchez, R. Control of cellular proliferation by modulation of oxidative phosphorylation in human and rodent fast-growing tumor cells. *Toxicol. Appl. Pharmacol.* **2006**, *215*, 208–217. [CrossRef]
77. Bravo-Gómez, M.E.; Campero-Peredo, C.; García-Conde, D.; Mosqueira-Santillán, M.J.; Serment-Guerrero, J.; Ruiz-Azuara, L. DNA-Binding Mode of Antitumoral Copper Compounds (Casiopeínas®) and Analysis of its Biological Meaning. *Polyhedron* **2015**, *102*, 530–538. [CrossRef]
78. Serment-Guerrero, J.; Cano-Sanchez, P.; Reyes-Perez, E.; Velazquez-Garcia, F.; Bravo-Gomez, M.E.; Ruiz-Azuara, L. Genotoxicity of the copper antineoplastic coordination complexes Casiopeínas. *Toxicol. In Vitro* **2011**, *25*, 1376–1384. [CrossRef] [PubMed]
79. Ruiz-Azuara, L.; Bastian, G.; Bravo-Gómez, M.E.; Cañas, R.C.; Flores-Alamo, M.; Fuentes, I.; Mejia, C.; García-Ramos, J.C.; Serrano, A. Abstract CT408: Phase I study of one mixed chelates copper(II) compound, Casiopeína CasIIIia with antitumor activity and its mechanism of action. *Cancer Res.* **2014**, *74*, 19.
80. Krasnovskaya, O.; Naumov, A.; Guk, D.; Gorelkin, P.; Erofeev, A.; Beloglazkina, E.; Majouga, A. Copper Coordination Compounds as Biologically Active Agents. *Int. J. Mol. Sci.* **2020**, *21*, 3965. [CrossRef]
81. McGivern, T.; Afsharpour, S.; Marmion, C.J. Copper Complexes as Artificial DNA Metallonucleases: From Sigman's Reagent to Next Generation Anti-Cancer Agent? *Inorg. Chim. Acta.* **2018**, *472*, 12–39. [CrossRef]
82. Griffin, E.; Levina, A.; Lay, P.A. Vanadium(V) tris-3,5-di-tert-butylcatecholato complex: Links between speciation and anti-proliferative activity in human pancreatic cancer cells. *J. Inorg. Biochem.* **2019**, *201*, 110815. [CrossRef]
83. Chaudhary, A.; Singh, A.; Rawat, E.; Singh, R.V. Heterobimetallic Complexes: A Window into Medicinal Chemistry. *Chem. Sci. Rev. Lett.* **2016**, *5*, 98–119.
84. Rozzo, C.; Sanna, D.; Garribba, E.; Serra, M.; Cantara, A.; Palmieri, G.; Pisano, M. Antitumoral effect of vanadium compounds in malignant melanoma cell lines. *J. Inorg. Biochem.* **2017**, *174*, 14–24. [CrossRef]
85. Pisano, M.; Arru, C.; Serra, M.; Galleri, G.; Sanna, D.; Garribba, E.; Palmieri, G.; Rozzo, C. Antiproliferative activity of vanadium compounds: Effects on the major malignant melanoma molecular pathways. *Metallomics* **2019**, *11*, 1687–1699. [CrossRef]
86. Scibior, A.; Pietrzyk, L.; Plewa, Z.; Skiba, A. Vanadium: Risks and possible benefits in the light of a comprehensive overview of its pharmacotoxicological mechanisms and multi-applications with a summary of further research trends. *J. Trace Elem. Med. Biol.* **2020**, 126508. [CrossRef]